arXiv:cond-mat/0510739 v2 13 Jun 2006

Localisation versus self-trapping: Polaron formation in the Anderson-Holstein model

Holger Fehske, Franz X. Bronold, and Andreas Alvermann

Institut für Physik, Ernst-Moritz-Arndt-Universität Greifswald, 17487 Greifswald, Germany

1. – Problem

The polaron concept, first introduced by Landau [1], is one of the main pillars on which the theoretical analysis of materials with strong electron-phonon (EP) coupling rests. In these compounds, the coupling between the electron and the lattice leads to a lattice deformation whose potential tends to bind the electron to the deformed region of the crystal. This process, which has been called self-trapping because the potential depends on the state of the electron, does not destroy translational invariance, even if the lattice deformation is confined to a single lattice site (small polaron) [2, 3]. Quantum mechanical tunnelling between different lattice sites restores this symmetry and ensures that a self-trapped electron forms an itinerant polaronic quasi-particle-particle.

In contrast to a weakly phonon-dressed electron, a polaron is strongly mass-enhanced, because of the lattice distortion it has to coherently carry along. A polaron is therefore rather sluggish and accordingly susceptible to random changes in the local environment. Crystallographic and chemical defects may easily turn an itinerant polaron into a localised particle which is confined to a finite region of the crystal. This confinement can arise as the polaron binds to an impurity which is energetically separated from the band of itinerant states. More interestingly the scattering on defects can lead to destructive interference which transmutes an itinerant state to a localised state. This transmutation is called Anderson localisation [4, 5]. It is as central to the analysis of disordered materials as the polaron concept is for materials with strong EP coupling.

An electron in a localised state is of course strongly coupled to local lattice distortions.

© Società Italiana di Fisica

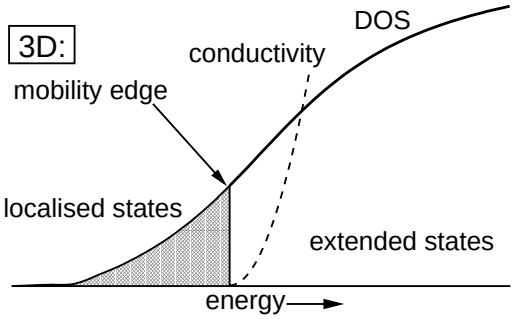

Fig. 1. – The figure displays the density of states (DOS) for the single-electron Anderson model. States deep inside the band are extended, whereas states below (above) the lower (upper) mobility edge are localised. The dc-conductivity vanishes at the mobility edge. Note that the DOS is finite in the region of localised states.

Anderson localisation and self-trapping are thus intricately connected. Yet, a combined analysis of the two is, with a few exceptions [6–9], conspicuously missing in the polaron literature. This is a serious shortcoming because a priori it is not clear whether Anderson localisation and self-trapping always work in the same direction, as suggested by the simple discussion given above.

The purpose of this contribution is to describe a theoretical approach capable of accounting for both Anderson localisation and self-trapping, and to apply it to the analysis of the issue just mentioned. We present precise criteria to distinguish itinerant from localised polarons. With these criteria at hand we study the localisation behaviour of a single polaron in dependence on the EP coupling.

2. – Modelling

To discuss the interplay of EP coupling and randomness, let us consider, as a generic model, the single-particle Anderson-Holstein Hamiltonian

$$H = \sum_i \epsilon_i n_i - t \sum_{\langle i,j \rangle} c_i^\dagger c_j - \sqrt{\varepsilon_p \omega_0} \sum_i (b_i^\dagger + b_i) n_i + \omega_0 \sum_i b_i^\dagger b_i \ , \tag{1}$$

where t is the electron transfer amplitude between neighbouring sites on a three-dimensional (3D) lattice, ω_0 is the bare phonon frequency ($\hbar = 1$), ε_p is the polaron shift, and $n_i = c_i^\dagger c_i$ is the local charge density. The on-site energies $\{\epsilon_i\}$ are independently identically distributed random variables with common distribution $P(\epsilon_i) = \frac{1}{\gamma}\theta\left(\frac{\gamma}{2} - |\epsilon_i|\right)$.

Without EP coupling ($\varepsilon_p = 0$), i.e. for a bare electron in a disordered 3D crystal, Anderson has shown that all states are localised provided the width γ of the distribution of the on-site energies ϵ_i exceeds a critical value γ_c [4]. When $\gamma < \gamma_c$, electron states towards the band edges would be localised in this model whereas states towards the band centre would be extended (and thus itinerant). Mobility edges at $\pm\omega_{\rm mob}(\gamma)$ separate the two classes of electron states [10] (see Fig. 1). We will be only concerned with this 3D setting: In 1D (and arguably 2D) tight-binding models with random on-site energies all states are localised no matter how small γ.

3. – Stochastic Green's function approach

The most natural quantity to characterise the localisation of a bare electron is the localisation length l defined by $|\psi(\mathbf{r})| \propto \exp(-r/l)$, where $\psi(\mathbf{r})$ is the electron wave-function at energy ω. If l diverges (is finite), the state is extended (localised). In most cases of interest, however, the wave-function cannot be straightforwardly determined. Alternative quantities suitable for a theoretical analysis are the (disorder averaged) $T = 0$ dc-conductivity which is finite only for extended states, or the $T = 0$ return-probability which is finite only for localised states. Both quantities are four-point correlation functions and thus also hard to obtain. Two-point functions, for instance the local density of states (LDOS),

$$\rho_i(\omega) = \sum_n |\psi_n(\mathbf{r}_i)|^2 \delta(\omega - E_n) = -\frac{1}{\pi} \mathrm{Im}\, G_{ii}(\omega) \tag{2}$$

($G_{ii}(\omega)$ is the local Green's function), are much easier to calculate but then disorder averaging is inappropriate: The (arithmetically averaged) DOS

$$\rho_{\mathrm{av}}(\omega) = \langle \rho_i(\omega) \rangle = \int \rho_i P[\rho_i(\omega)]\, d\rho_i \tag{3}$$

gives the number of states at ω independent of whether they are extended or localised.

It was Anderson who pointed out that in a disordered system one must study the *distribution* of such two-point functions [4]. From the distribution $P[\rho_i(\omega)]$ of the LDOS one can decide whether the state at energy ω is localised or not. For the ordered system $\rho_i(\omega)$ does not depend on i due to translational symmetry, and $P[\rho_i(\omega)] = \delta[\rho_i - \rho(\omega)]$. When, in an extended state, the electron wave-function has more or less equal weight on every lattice site, $P[\rho_i(\omega)]$ is rather symmetric and usually Gaussian. With increasing disorder, the weight of the wave-function becomes more and more restricted to a few lattice sites leading to a broad and asymmetric distribution (see left lower panel in Fig. 3 below). Above the localisation transition, the wave-function has appreciable weight only in a finite region. Thus, the distribution $P[\rho_i(\omega)]$ is singular, i.e. $P[\rho_i(\omega)] = \delta[\rho_i]$, signalling a localised state at energy ω.

To analyse the effects of disorder on polaron formation on the level of two-point functions we applied the recently developed statistical dynamical mean field theory (statDMFT) [11] to the Anderson-Holstein model. The statDMFT is a stochastic Green's function approach, based on the self-consistent construction of random samples (and thus distributions) for local Green's functions. Conceptually, it is an extension of the self-consistent theory of localisation of bare electrons [12] to models with interactions and has been successfully applied to the disordered Hubbard [11, 13], Anderson lattice [14], and Holstein models [15, 16].

The statDMFT maps the original lattice on to an ensemble of impurity sites each of which is self-consistently embedded in an effective medium comprising the environment of this site (cf. Fig. 2). The main approximation is to treat interaction processes as

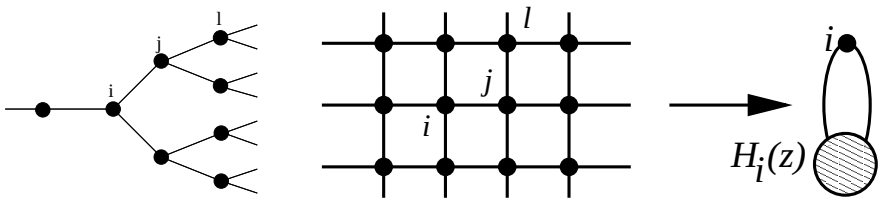

Fig. 2. – Philosophy of the statDMFT: The lattice problem is mapped on to an ensemble of impurity problems, each consisting of a single site i self-consistently embedded in an effective medium described by the hybridisation function $H_i(z)$; all lattice information is contained in this function. For a Bravais lattice the mapping leads to rather complicated equations. The statDMFT construction is therefore done for a Bethe lattice, shown on the very far left, where the fact that site i cannot be reached from l once j is removed leads to dramatic simplifications.

in conventional dynamical mean field theory (DMFT). Within this approximation EP coupling gives rise to a local self-energy $\Sigma_i(z)$ only. For a single electron in the Anderson-Holstein model $\Sigma_i(z)$ becomes a continued fraction [17]

$$\Sigma_i(z) = \cfrac{1\varepsilon_p\omega_0}{z - 1\omega_0 - \epsilon_i - H_i(z-1\omega_0) - \cfrac{2\varepsilon_p\omega_0}{z - 2\omega_0 - \epsilon_i - H_i(z-2\omega_0) - \cfrac{3\varepsilon_p\omega_0}{\cdots}}} \tag{4}$$

with $z = \omega + i\eta$ and the hybridisation function $H_i(z) = t^2 \sum_j G_{jj}(z)$. The index j runs over the K sites neighbouring to i, when K is the connectivity of the lattice. The K Green's functions $G_{jj}(z)$ in this sum have to be evaluated for a lattice with site i removed.

With this self-energy the local Green's function $G_{ii}(z)$ of the single-electron Anderson-Holstein model at $T = 0$ is given by

$$G_{ii}(z) = \frac{1}{z - \epsilon_i - H_i(z) - \Sigma_i(z)} \tag{5}$$

with a local contribution $\epsilon_i - \Sigma_i(\omega)$, and $H_i(z)$ accounting for the hopping to neighbouring sites. Apart from the DMFT treatment of interaction these equations are exact on a Bethe lattice where the removal of sites preserves the lattice structure. The details of the derivation are given in Ref. [16].

The ensemble of impurity sites is then analysed in terms of probability distributions. Due to the randomness of the on-site energies, $G_{ii}(z)$ is a random variable whose distribution function has to be numerically determined from Eq. (5). Towards that end, we proceed as follows: First, we reinterpret the site indices as labels enumerating the N elements of a random sample; each $G_{ii}(z)$, $i = 1, \cdots, N$, can be understood as a particular realisation of a random variable. We then self-consistently construct the random sample $\{G_{ii}(\omega)\}$, starting from an initial random sample, which we successively update

via a Monte Carlo sampling algorithm, drawing the random variables on the right habd side of Eq. (5) from the corresponding random samples created the iteration step before. Because in Eq. (4) $G_{jj}(\omega - p\omega_0)$ appears we have to simultaneously construct a random sample for all $G_{ii}(\omega - p\omega_0)$, with $p = 0, \cdots, M$, where M is the truncation depth of the continued fraction.

For reasonable numerical accuracy, the sample size N, which should not be confused with the actual size of the Bethe lattice but instead gives the precision with which we construct the random sample, has to be sufficiently large. Typical sample sizes are $N \approx 50\,000$. The depth M of the continued fraction, which describes the maximum number of virtual phonons in the lattice, has to be large enough in order to capture polaron formation. As a rough estimate we use $M \approx 5g^2$, where $g^2 = \varepsilon_p/\omega_0$ is approximately the average number of virtual phonons comprising the phonon cloud of the polaron.

From the self-consistent sample for $G_{ii}(z)$ we can directly read off the distribution for $\rho_i(\omega)$ in the form of a histogram. Instead of dealing with the full distribution we can characterise its deviation from a Gaussian reasonably well by a 'typical' value which is the geometric average of the random quantity, i.e.

$$\rho_{\rm ty}(\omega) = \exp\left[\int \ln(\rho_i) P[\rho_i(\omega)]\, d\rho_i\right] . \tag{6}$$

In the following we classify therefore states at energy ω as localised (extended) if the typical value $\rho_{\rm ty}(\omega)$ vanishes (is finite) and the average $\rho_{\rm av}(\omega)$ is finite. The latter condition ensures that there is a state at energy ω.

4. – Limiting cases

For the free electron, with $\epsilon_i = 0$ and $\Sigma_i = 0$, Eq. (5) is a quadratic equation whose solution provides the semi-circular DOS $\rho(\omega) = (4/\pi W_0^2)\sqrt{W_0^2 - 4\omega^2}$ of the Bethe lattice, with bare bandwidth $W_0 = 4t\sqrt{K}$. In what follows, we set $W_0 = 1$ on a $K = 2$ Bethe lattice and measure energies in units of W_0, defining the dimensionless parameters disorder strength $\bar{\gamma} = \gamma/W_0$, EP coupling constants $\bar{\lambda} = 2\varepsilon_p/W_0$ and $g^2 = \varepsilon_p/\omega_0$, and phonon frequency $\bar{\omega}_0 = \omega_0/W_0$.

4˙1. *Anderson model.* – Let us first discuss the bare Anderson model ($\bar{\lambda} = 0$), when our approach reduces to the self-consistent theory of localisation [12]. Then we can determine the mobility edge trajectory for a single electron on the $K = 2$ Bethe lattice.

For a qualitative discussion of the localisation behaviour, it is sufficient to obtain random samples for a small but finite imaginary part of $z = \omega + \mathrm{i}\eta$. If not stated otherwise, $\eta = 10^{-8}$. For a quantitative determination of mobility edges it is necessary, however, to track the average and typical LDOS for $\eta \to 0$. The fingerprint of a localised state at energy ω is a finite $\rho_{\rm av}(\omega)$ and a vanishing $\rho_{\rm ty}(\omega)$ for $\eta \to 0$ (see right panel in Fig. 3). In the upper left panel of Fig. 3 we present the mobility edge trajectory for a single electron in the Anderson model obtained this way.

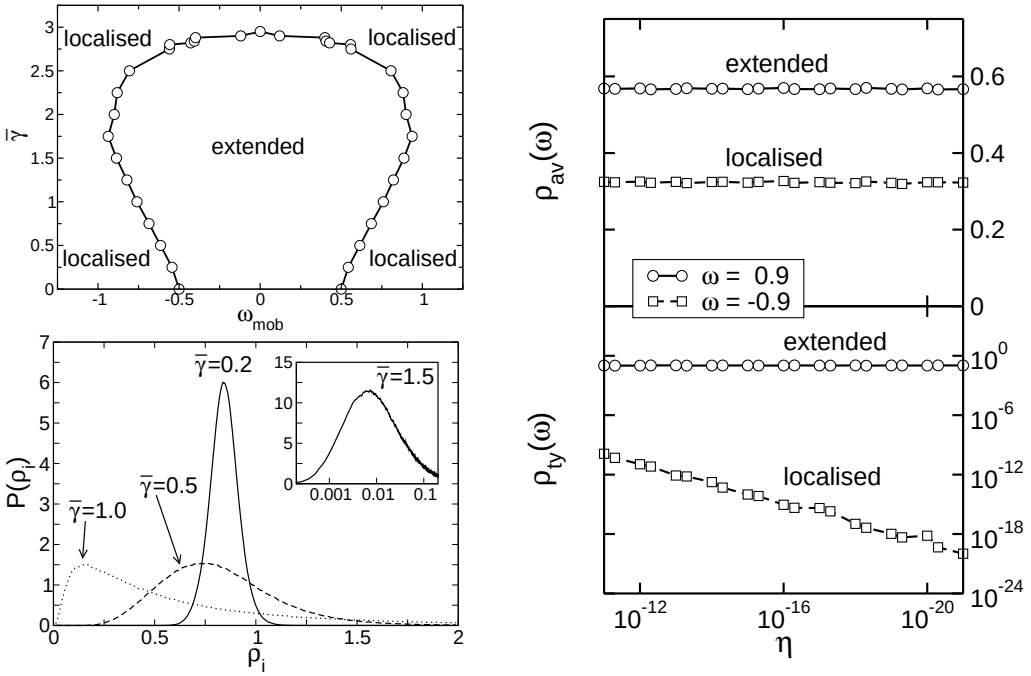

Fig. 3. – The upper left panel depicts the mobility edge trajectory for a single electron in the bare Anderson model. The lower left panel gives the distribution $P[\rho_i(\omega = 0)]$ for different $\bar{\gamma}$. The right panel shows the behaviour of the averaged and typical LDOS for extended and localised states in the limit $\eta \to 0$ ($\bar{\gamma} = 1.5$).

Obviously, our approach is accurate enough to detect the two competing effects associated with the characteristic re-entrance behaviour of the mobility edge trajectory: The formation of delocalised states in the vicinity of the band edge at small disorder and the localisation transition at large disorder [5]. Even in the strongly disordered regime, where the mobility edges move to the centre of the band and all states are localised, the statDMFT works reliably well. We did not attempt to estimate the statistical error, but it should be of the order of the fluctuations visible in the plot. By its construction on a Bethe lattice, and in view of the localisation behaviour obtained, the statDMFT comprehensively describes localisation in a 3D system. The localisation behaviour in 1D and 2D is, in accordance with the goal of our studies, beyond the scope of this approach.

4˙2. *Holstein model.* – For $\gamma = 0$, our approach reduces to the DMFT of a single polaron in the Holstein model [17], the physical properties of which are governed by two parameter ratios: The adiabaticity ratio $\bar{\omega}_0$ and the dimensionless EP coupling constants $\bar{\lambda}$ and g^2. Polaron formation sets in if both $\bar{\lambda} > 1$ and $g^2 > 1$.

The left panel of Fig. 4 illustrates the on-set of polaron formation with increasing EP coupling. The DOS fragments into an increasing number of sub-bands, and a new energy scale arises: The strongly renormalised width W of the polaronic sub-bands. As

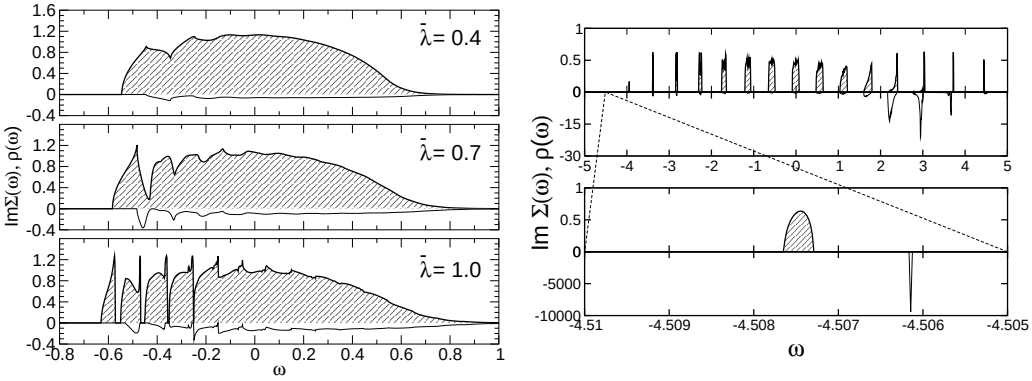

Fig. 4. – Left panel: Evolution of the DMFT DOS (thick solid line) and the imaginary part of the interaction self-energy (thin solid line) for the Holstein model with $\bar{\omega}_0 = 0.1$ and increasing EP coupling $\bar{\lambda} = 0.4, 0.7$, and 1.0. Right panel: DMFT DOS and imaginary part of the interaction self-energy in the anti-adiabatic strong-coupling regime ($\bar{\omega}_0 = 0.5625$ and $\bar{\lambda} = 9.0$). The lower panel shows the extremely narrow lowest sub-band ($W = 3.45 \times 10^{-4}$) in more detail.

far as localisation is concerned, the lowest sub-band is particularly important, because it is completely coherent ($\mathrm{Im}\,\Sigma_i(\omega) = 0$) and inelastic scattering does not mask the localisation process. The internal structure of the states of the lowest sub-band depends on $\bar{\lambda}$ and $\bar{\omega}_0$. For the adiabatic polaron, shown in the left panel of Fig. 4, this gives rise to a pronounced asymmetry in the DOS (provided $\bar{\lambda}$ is not too large). Specifically the states at the top of the lowest sub-band are phonon dominated leading to a substantial band flattening. States at the bottom of the sub-band have a smaller phonon admixture. These states are more mobile as compared to a rescaled tight-binding electron due to long-range tunnelling processes induced by EP coupling [18]. Both, band flattening and long-range tunnelling will of course affect the localisation behaviour of a polaron. In contrast, the composition of the states of the lowest sub-band is more or less homogeneous in the anti-adiabatic strong-coupling regime shown in the right panel of Fig. 4 . Self-trapping leads here to a band collapse resulting in an extremely narrow sub-band whose DOS is essentially identical to the rescaled semi-circular DOS of the Bethe lattice.

4˙3. *Infinite dimension.* – DMFT becomes exact if the lattice has infinite connectivity. In the limit $K \to \infty$ we have to re-scale the transfer amplitude as $t \to \bar{t}/\sqrt{K}$ to keep the bandwidth $W_0 = 4t\sqrt{K}$ constant. Applying the central limit theorem to $H_i(z)$ we find that $H_i(z)$ converges to its arithmetic mean (average value). The configuration average of Eq. (5) is then only a simple single-site average over ϵ_i and leads to a closed system of equations – precisely the DMFT equations – for the averaged local Green's function $G_{\mathrm{av}}(z)$. Each impurity site experiences in this limit the same environment. Disorder is thus only treated at the level of the coherent potential approximation and localisation cannot be detected. Note that the statDMFT, instead, keeps K finite. Hence, the environment of each impurity site is allowed to fluctuate leading to Anderson localisation

provided the fluctuations are strong enough.

5. – Anderson-Holstein model

We now turn our attention to the combined effect of disorder and EP coupling. At weak enough EP coupling, where the mean free path due to inelastic EP scattering is shorter than the localisation length, EP coupling suppresses localisation [19]. Phonons act then only as scattering centres which randomly change the phase of the electron wave-function before destructive interference due to elastic electron-impurity scattering – being essential for Anderson localisation – can occur. In the strong EP coupling regime, however, the DOS of the clean system fragments into polaronic sub-bands (Fig. 4), the lowest of which turns out to be completely coherent. States comprising this sub-band suffer no inelastic scattering – an ideal situation for destructive interference and thus for Anderson localisation. Because it is also much narrower than the bare electron band, extremely small amounts of disorder would suffice to localise states within this sub-band.

Obviously, the spread $\bar{\gamma}$ of the on-site energies ϵ_i can be small on the scale of the bare bandwidth but large on the scale of the width of the sub-bands. In the Anderson-Holstein model, we have to distinguish therefore at least between two regimes: The *Holstein regime*, where disorder is small on the scale of the bare bandwidth, and the *Anderson regime*, where it is large on the scale of the width of the polaronic sub-bands.

5˙1. *Anderson regime*. – First we consider the Anderson regime. In addition to the LDOS $\rho_i(\omega)$, the statDMFT suggests to use the imaginary part of the hybridisation function, the escape rate from a given site $\Gamma_i(\omega) = -\mathrm{Im}\, H_i(\omega)/\pi$, to characterise the localisation behaviour of a state at energy ω. Obviously, a finite (vanishing) escape rate $\Gamma_i(\omega)$ implies an extended (localised) state at energy ω. Similar to the LDOS $\rho_i(\omega)$ we have to consider its typical value $\Gamma_{\mathrm{ty}}(\omega)$.

The left panel of Fig. 5 displays typical escape rates as a function of $\bar{\gamma}$ for two energies, one below and one above the phonon emission threshold (see inset). Below the threshold, $\mathrm{Im}\Sigma_i(\omega) = 0$, and the states are coherent. Anderson localisation occurs at the value $(\bar{\gamma}_c)_{\omega=-0.4} \approx 2.25$ for which $\Gamma_{\mathrm{ty}}(\omega)$ vanishes. Since the phonon dressing of these states is negligible the escape rates of the interacting and non-interacting system vanish at roughly the same $\bar{\gamma}_c$. Above the threshold, inelastic EP scattering ($\mathrm{Im}\,\Sigma_i(\omega) \neq 0$) disrupts the destructive interference required for localisation. Here, the critical disorder strength $(\bar{\gamma}_c)_{\omega=0.4} \approx 3.0$ for which $\Gamma_{\mathrm{ty}}(\omega)$ vanishes is larger than below the phonon emission threshold. Thus, above the threshold, localisation is suppressed. It is rather encouraging that our approach recovers this basic feature of the physics of localisation.

In the right panel of Fig. 5 we show the typical LDOS together with the DMFT DOS for $\bar{\omega}_0 = 0.05$, $\bar{\lambda} = 1.0$, and $\bar{\gamma} = 2$. Without EP coupling, there would be mobility edges at $\omega \approx \pm 0.9$ (see Fig. 3). In the presence of EP coupling, the lower mobility edge is still located at the mobility edge of the noninteracting system, but the upper mobility edge is shifted to higher energies. Thus, precisely at the upper mobility edge EP coupling delocalises states.

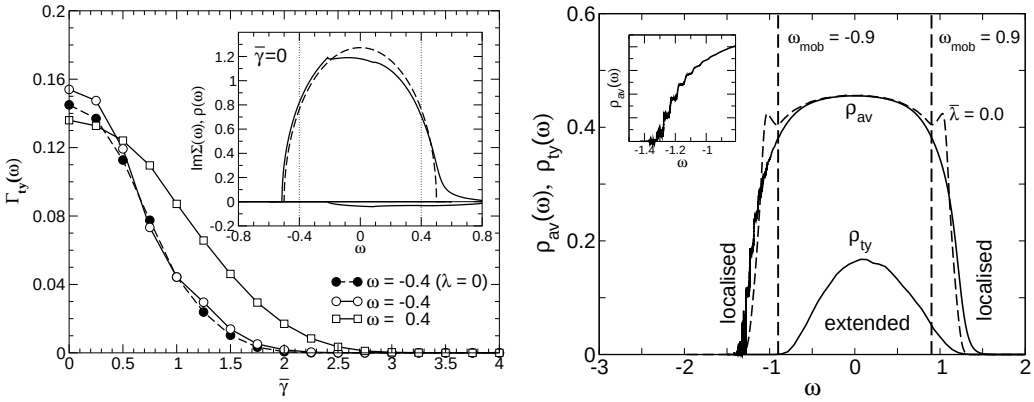

Fig. 5. – Left panel: Typical escape rate in the Anderson regime for weak EP coupling ($\bar{\lambda} = 0.067$ and $\bar{\omega}_0 = 0.3$). Filled circles denote data for $\bar{\lambda} = 0$. The inset shows the DMFT DOS and the imaginary part of the interaction self-energy for $\bar{\gamma} = 0$, as well as the bare DOS for $\bar{\lambda} = \bar{\gamma} = 0$ (dashed line). Vertical dotted lines indicate the energies for which the escape rate is plotted. Right panel: Typical LDOS and DMFT DOS in the Anderson regime for intermediate EP coupling ($\bar{\lambda} = 1.0$, $\bar{\omega}_0 = 0.05$, and $\bar{\gamma} = 2$). The dashed line depicts the averaged LDOS for $\bar{\lambda} = 0$. Vertical dashed lines indicate the mobility edges of the noninteracting system; the inset displays the DMFT DOS at the left band edge.

To explain this asymmetry, recall that our calculation is for $T = 0$. Hence, states at energy ω can, due to EP interaction, only couple to states at energies less than ω. At the high energy side localised states above the mobility edge of the noninteracting system couple to delocalised states below. As a consequence, formerly localised states become delocalised. In contrast, states below the lower mobility edge of the noninteracting system remain localised, because they can only couple to states which are already localised. Additionally, EP interaction attempts to transform electronic band states above the lower mobility edge of the noninteracting system into polaronic states, as suggested by Anderson [6]. Hence, these states become heavier and more susceptible to disorder. As a result, at the lower mobility edge EP coupling enhances the tendency towards localisation.

Let us take a closer look at the DMFT DOS, which at the low-energy side shows pronounced plateaus with a width given by the phonon energy. This step-like increase of the DOS, together with the vanishing of the typical LDOS, is a clear signature for localised polaronic defect states. Being strongly localised these states can be described by the independent boson model whose density of states consists of discrete peaks separated by ω_0. The DOS does not change with energy as long as the fluctuations of the on-site energies are smaller than the phonon energy. If the difference in on-site energy is equal to the phonon energy, a step arises because states with one additional phonon contribute. The step height reflects therefore the phonon distribution of the polaronic defect states.

Our approach identifies the mobility edge which separates, in the strongly disordered Anderson regime, polaronic defect states from itinerant polarons. This is a fundamental first step towards a microscopic theory of polaron transport in disordered media which,

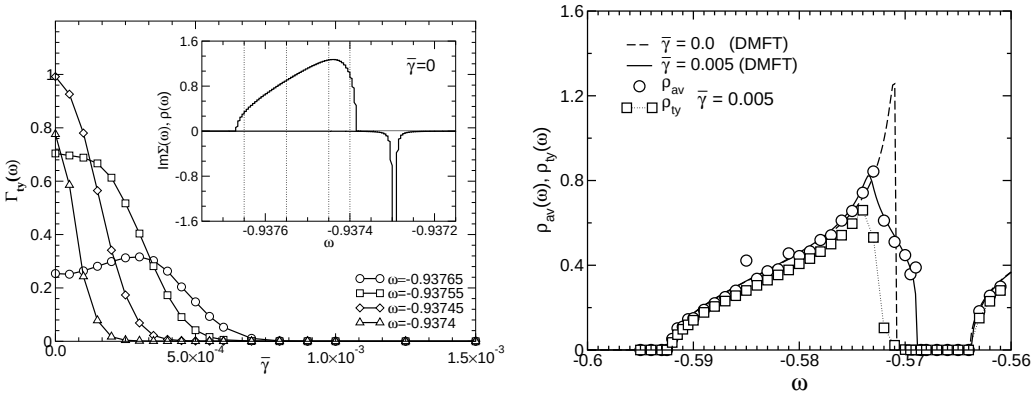

Fig. 6. – Left panel: Typical escape rates in the adiabatic intermediate-to-strong coupling regime ($\bar{\omega}_0 = 0.1$, $\bar{\lambda} = 1.8$). The inset displays the DMFT DOS for the lowest sub-band and the imaginary part of the interaction self-energy for $\bar{\gamma} = 0$; vertical dotted lines indicate the energies for which $\Gamma_{\rm ty}(\omega)$ is plotted. Right panel: Average and typical LDOS in the polaron cross-over regime ($\bar{\omega}_0 = 0.0625$, $\bar{\lambda} = 1.0$) for $\bar{\gamma} = 0.005$. Note, the average LDOS is almost perfectly approximated by the DMFT DOS. At about $\omega = -0.565$ the second polaronic sub-band starts.

in principle, could cover thermally activated hopping between polaronic defects below the mobility edge.

5˙2. *Holstein regime.* – In the Holstein regime the spread of the on-site energies is much smaller than the bare bandwidth. We only consider the situation where $\bar{\gamma}$ is so small that disorder cannot mix different polaronic sub-bands. In that case, mobility edges within the lowest sub-band can be identified and tracked as a function of disorder.

In the left panel of Fig. 6 we present typical escape rates as a function of $\bar{\gamma}$ for the lowest polaronic sub-band. In the adiabatic intermediate-to-strong coupling regime, the DMFT DOS (for $\bar{\gamma} = 0$, inset of Fig. 6) is rather asymmetric because of the 'hybridisation' with the (optical) phonon branch, leading to band flattening. As a result, states at the top of the sub-band are very susceptible to disorder and the critical disorder strength for which $\Gamma_{\rm ty}(\omega)$ vanishes is substantially smaller than at the bottom of the sub-band. Clearly, in contrast to the bare Anderson model, there is a significant asymmetry of the localisation behaviour of the states within the sub-band. To demonstrate the effect of this asymmetry more clearly, we plot in the right panel of Fig. 6 the typical and average LDOS for the lowest sub-band in the adiabatic cross-over regime for $\bar{\gamma} = 0.005$. The steeple-like shape due to band flattening is now very pronounced and the suppression of the typical LDOS at the top of the sub-band can be clearly seen.

The same asymmetry is manifest in the mobility edge trajectory for the lowest sub-band in the adiabatic cross-over regime, which we partly show in Fig. 7. As expected, states at the bottom of the sub-band are almost insensitive to small amounts of disorder. The lower mobility edge (and also the lower band edge) is essentially pinned. Notice, in this regime polaron states at the bottom of the sub-band are even more difficult to

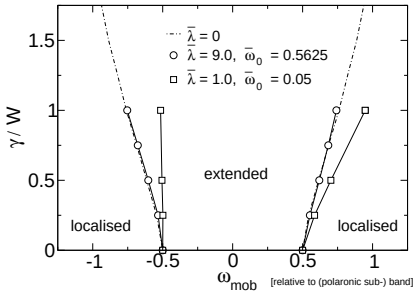

Fig. 7. – Parts of the mobility edge trajectory for the lowest polaronic sub-band of the Anderson-Holstein model in the adiabatic cross-over ($\bar{\omega}_0 = 0.05$ and $\bar{\lambda} = 1$, □) and the anti-adiabatic strong coupling regime ($\bar{\omega}_0 = 0.5625$ and $\bar{\lambda} = 9$, ○). Disorder is measured in units of the respective width W of the sub-bands, and $\omega_{\rm mob}$ is given relative to the sub-band position. The mobility edge trajectory for the bare Anderson model (dashed-dotted line) is given for comparison.

localise than bare electron states if we measure the disorder on the relevant energy scale W or W_0, respectively. Thus, even in absence of the suppression of localisation due to inelastic scattering, a polaron is not always easier to localise than an electron. States at the top of the sub-band, on the other hand, are immediately affected by disorder. Small amounts of disorder (small even on the scale of the sub-band) are sufficient to localise the states, and the upper mobility edge rapidly shifts to higher energies.

For (large) disorder disorder $\gamma \gtrsim W$, the upper band edge of the disorder-broadened lowest sub-band moves into a spectral range with significant inelastic scattering (not shown in Fig. 7). The enhanced inelastic scattering rate for the states at the top of the lowest sub-band strongly suppresses localisation in this spectral range. With increasing disorder states move into the gap region, which separates the first from the second sub-band, thereby giving rise to a shrinking gap. Finally both sub-bands merge. This redistribution of states occurs before a re-entrance behaviour of the mobility edge trajectories can be observed.

Also shown in Fig. 7 is the mobility edge trajectory for the lowest sub-band in the anti-adiabatic strong-coupling regime ($\bar{\omega}_0 = 0.5625$ and $\bar{\lambda} = 9$). Here self-trapping manifests itself in a very narrow coherent band which is essentially a rescaled replica of the bare band. The localisation properties of the lowest sub-band in the anti-adiabatic strong-coupling regime are therefore those of a rescaled Anderson model as can be seen from the perfect match of the properly scaled mobility edge trajectories.

6. – Conclusions

Based on a stochastic Green's function approach we analysed, for representative situations, the interplay between Anderson localisation and self-trapping in the framework of the Anderson-Holstein model.

Only in the anti-adiabatic Holstein regime the localisation properties are essentially those of a rescaled Anderson model whereas they are strongly affected by the internal structure of the phonon dressing in all other cases. As demonstrated EP coupling can either work against localisation due to inelastic scattering, or enhance the tendency towards localisation due to self-trapping. A polaron can be rather easy to localise with respect to the energy scale set by EP coupling (e.g. the width of the lowest polaronic sub-band) – but notably, also in regions without inelastic scattering, it can be even harder

to localise than the bare electron. Most importantly, EP coupling can change localised electron states to strongly localised polaronic defect states. Transport between these states has to occur by thermally activated hopping. Our approach, which is capable to track this transmutation, should be thus suitable for investigating the cross-over from hopping transport below the lower mobility edge to band transport above it.

Our investigation of the Anderson-Holstein model is far from being complete. For instance, a systematic study of the parameter range where disorder mixes polaronic sub-bands has not yet been done, as well as an investigation at finite temperatures or particle densities. In particular the latter is rather complicated because the EP self-energy can then be no longer analytically obtained in the form of a continued fraction. Most pressing, however, is the calculation of the finite temperature conductivity for a single polaron because it would open the door to a microscopic theory of polaron transport. Preliminary work in this direction exists only without disorder [20], which is however crucial for a complete description of polaron transport.

REFERENCES

[1] Landau L.D., *Z. Phys.*, **3** (1933) 664.
[2] Firsov Y.A., *Polarons* (Izd. Nauka, Moscow), 1975; Emin D., in *Polarons and bipolarons in High-T_c superconductors and related materials*, edited by E.K.H. Salje, A.S. Alexandrov and W.Y. Liang (Cambridge University Press, Cambridge), 1995.
[3] Fehske H., Alvermann A., Hohenadler M., and Wellein G., Proc. Int. School of Physics "Enrico Fermi", Course CLXI, *Polarons in Bulk Materials and Systems with Reduced Dimensionality*, Eds. G. Iadonisi, J. Ranninger, G. de Filippis, (IOS Press, Amsterdam, Oxford, Tokio, Washington DC) 2006, pp 285-296.
[4] Anderson P.W., *Phys. Rev.*, **109** (1958) 1492.
[5] Kramer B. and MacKinnon A., *Rep. Prog. Phys.*, **56** (1993) 1469.
[6] Anderson P.W., *Nature*, **235** (1972) 163.
[7] Girvin S.M. and Jonson M., *Phys. Rev. B*, **22** (1980) 3583.
[8] Mueller H. and Thomas P., *Phys. Rev. Lett.*, **51** (1983) 702.
[9] Cohen M.H., Economou E.N. and Soukoulis C.M., *Phys. Rev. Lett.*, **51** (1983) 1202.
[10] Mott N.F., *Philos. Mag.*, **13** (1966) 989.
[11] Dobrosavljević V. and Kotliar G., *Phys. Rev. Lett.*, **78** (1997) 3943.
[12] Abou-Chacra R., Anderson P.W. and Thouless D.J., *J. Phys. C*, **6** (1973) 1734.
[13] Dobrosavljević V. and Kotliar G., *Phil. Trans. R. Soc. Lond. A*, **356** (1998) 57.
[14] Aguiar M.C.O., Miranda E. and Dobrosavljević V., *Phys. Rev. B*, **68** (2003) 125104.
[15] Bronold F.X. and Fehske H., *Phys. Rev. B*, **66** (2002) 073102.
[16] Bronold F.X., Alvermann A. and Fehske H., *Philos. Mag.*, **84** (2004) 673.
[17] Sumi H., *J. Phys. Soc. Jpn.*, **36** (1974) 770; Ciuchi S., DePasquale F., Fratini S. and Feinberg D., *Phys. Rev. B*, **56** (1997) 4494; Ciuchi S., Capone M., Cappelluti E., and Sangiovanni G., Proc. Int. School of Physics "Enrico Fermi", Course CLXI, *Polarons in Bulk Materials and Systems with Reduced Dimensionality*, Eds. G. Iadonisi, J. Ranninger, G. de Filippis, (IOS Press, Amsterdam, Oxford, Tokio, Washington DC) 2006, pp 131-153.
[18] Wellein G. and Fehske H., *Phys. Rev. B*, **58** (1998) 6208.
[19] Lee P.A. and Ramakrishnan T.V., *Rev. Mod. Phys.*, **57** (1985) 287.
[20] Fratini S. and Ciuchi S., *Phys. Rev. Lett.*, **91** (2003) 256403; Schubert G., Wellein G., Weisse A., Alvermann A. and Fehske H., *Phys. Rev. B*, **72**, (2005) 104304.